ACS OMEGA

Open Access

http://pubs.acs.org/journal/acsodf

Article

ALTMAN: A Novel Method for Cell Cycle Analysis

Zining Wang, Tian Wang, Xiaohui Chen, Linxi Lv, Yang Luo,* and Wei Gu*

Cite This: *ACS Omega* 2024, 9, 37780−37788

Read Online

ACCESS | Metrics & More | Article Recommendations | Supporting Information

ABSTRACT: Accurate analysis of S-phase fraction is crucial for the assessment of cell proliferation levels, tumor malignancy and prognostic effects of treatment. Most of the currently developed methods for S-phase cell analysis rely on flow cytometric analysis of DNA content determination. However, the lack of standardized procedures for sample analysis and interpretation of cell cycle fitting graphs poses a significant limitation in clinical practice for utilizing flow cytometry to measure the cell cycle based on DNA content. Herein, we developed an approach for analyzing S-phase cells based on telomerase activity determination. Briefly, this approach distinguishes S-phase cells in cell populations via direct fluorescence tracking of telomerase activity within individual cells. The dynamic analysis of telomerase activity in different cell cycles was made possible by the ALTMAN strategy developed in our previous studies, which has been successfully employed to distinguish S-phase cells in cultured cells. This method offers a novel avenue for the assessment of cell cycle status and the evaluation of the proliferation status of tumor cells and the prognosis effect of tumor patients via analyzing the differences in telomerase activity during different cell cycle processes.

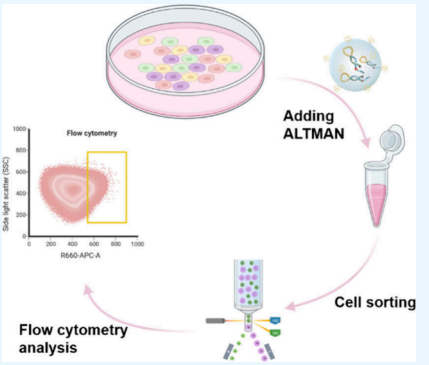

INTRODUCTION

The cell cycle is a tightly controlled process that enables all living organisms to grow and proliferate.[1] Since the early 1970s, the study of cell cycle regulation has gained significant attention, especially in the fields of stem cell and antitumor research.[2,3] In eukaryotic cells, the cell cycle consists of four distinct phases, namely the G1 phase, S phase, G2 phase, and M phase, which progress in a unidirectional manner.[4,5] Among these phases, the S-phase stage plays a critical role in DNA replication, the synthesis of chromatin proteins, and the formation of DNA into chromatin structures.[6−8] The frequency of S-phase cells, representing cells in the DNA synthesis phase, serves as a fundamental parameter in research related to the regulation of the cell division cycle and proliferation rates. It also aids in predicting tumor malignancy and reflects the kinetic law of tumor cell proliferation.[9−11]

The traditional methods of analyzing S-phase cell fraction include flow cytometry based on DNA content analysis. This method primarily determines S-phase fraction by modeling the distribution of 2N and 4N cells.[12,13] However, the lack of standardized procedures for sample analysis and interpretation of cell cycle fitting graphs has limited the practical clinical application of flow cytometry in cell cycle analysis.[14,15] Moreover, flow cytometry may present challenges in precisely distinguishing between cells in the G1/S and S phases due to difficulties in accurately assessing DNA content in living cells.[16] Although bivariate bromodeoxyuridine (BrdU)/DNA content analysis can reduce some uncertainties, denaturation of intracellular DNA is required for cell cycle analysis based on BrdU, which inducing the detected S-phase cells are difficult to further analyze and validate.[17,18] The fluorescent ubiquitination-based cell cycle indicator (FUCCI) method enables cell cycle analysis by labeling cell cycle-associated regulatory proteins with two-color fluorescent proteins.[19] However, fluorescence microscopy may not be able to simultaneously monitor other cellular processes when using this method, such as GFP-based fusion proteins, sensors, or genetically modified organisms. In addition, measuring cell division time by optical dynamic microscopy can exclude dead or noncycling cells to a certain extent, but this method is time-consuming and the cells are highly susceptible to phototoxic contamination.[20,21] Therefore, despite advances, the analysis of the fraction of S-phase cells remains challenging.

Telomerase is an enzyme that plays a crucial role in maintaining the length of telomeres, which are protective caps at the end of chromosomes.[22,23] The activity of telomerase is closely linked to the cell cycle, as it is primarily active during periods of cell division and growth.[24] Research has demonstrated disparities in telomerase activity across various phases of the cell cycle.[25,26] By measuring telomerase activity, researchers can gain insights into the status of the cell cycle, particularly in the highly activated state observed in the S-phase, as high levels of telomerase activity are typically associated with rapidly

Received: April 16, 2024
Revised: June 27, 2024
Accepted: July 11, 2024
Published: July 22, 2024

dividing cells. Therefore, detecting telomerase activity can serve as a useful tool for monitoring the progression of the cell cycle and understanding the dynamics of cell growth and division. Moreover, evaluating cell cycle status through the assessment of discrepancies in telomerase activity presents a novel avenue for prognostic assessment in tumors related to S-phase cell fraction.

Here, we employed ALTMAN, a telomerase activity assay developed by our research group in the early stage,[27] to analyze telomerase activity in different cell cycle phases. The ALTMAN approach Integrated the enzyme-free isothermal signal amplification, successfully increasing the sensitivity and reducing interference via leveraging the skillful design of the molecular beacon (MB) and the extension of the telomerase-activated TTAGGG repeat sequence. ALTMAN enabled ultrasensitive visualization of activated telomerase exclusively with a prominent detection limit of 2 cells·μL^{-1} and realized real-time imaging of telomerase activity in living cancer cells. MB of the ALTMAN approach has the advantages of high specificity, easy operation, and low signal-to-noise ratio, which can be used for the precise analysis of telomerase activity in individual cells. Therefore, the study utilized the ALTMAN strategy to analyze intracellular real-time telomerase activity during different cell cycle processes and further enabled S-phase cell sorting of cultured cell populations by distinguishing telomerase activity differences. This work provides a simple and efficient S-phase discrimination protocol as a prelude to accurate investigation of cell cycle-targeted tumor therapy and the assessment of the prognostic status of tumor patients treated.

EXPERIMENTAL SECTION

Materials and Apparatus. The oligonucleotides were synthesized and HPLC-purified by Sangon Biotechnology Co. Ltd. (China). The details of the synthesis MB sequence are as follows: MB (BHQ2-GACGGATTCCCTAACCC-TAAATCCGTCGA-Cy5-GCAGAGTT). L-mimosine, Thymidine, and Nocodazole were purchased from Sigma-Aldrich (China). Propidium iodide (PI), 4′,6-Diamidino-2-phenylindole (DAPI), and 4% Paraformaldehyde fix solution were obtained from Beyotime (China). 3′-Azido-3′-deoxythymidine (AZT), Trypsin, and thrombin (from human plasma) were bought from Solarbio Science & Technology Co, Ltd. (China). Bovine serum albumin (BSA) was obtained from Glenview (USA). cDNA reverse transcription kits and the fast qPCR master mix were bought from Sangon Biotech (China) and BBI Life Sciences Corporation (China). DMEM medium and Fetal bovine serum (FBS) were acquired from Gibco (USA). Dulbecco's modified Eagle's medium (DMEM) and penicillin−streptomycin were purchased from Hyclone (USA). Flow cytometric analyses were carried out on CytoFLEX Flow Cytometer (Beckman Coulter, USA) and BD FACSAria III Cell Sorter (BD Biosciences, USA). FI was measured using an Infinite 200 PRO (Tecan, Switzerland). Confocal laser scanning microscope (CLSM) images were captured by an LSM 980 SYSTEM (Zeiss, Germany). The materials for digital PCR, including the oil and amplification kit, were purchased from Bio-Rad, and the data were captured using a QX200 Droplet Digital PCR machine (Bio-Rad, USA). Live cell imaging was captured by the Nanolive (Bio-Rad, USA). All aqueous solutions employed in this experiment were meticulously prepared using ultrapure water, and all other chemicals utilized were of analytical grade.

Cell Culture and Telomerase Extraction. The cells utilized in this study were sourced from the Cell Bank of the Committee on Type Culture Collection of the Chinese Academy of Sciences. All types of cells were cultured in DMEM medium containing 10% FBS and 1% penicillin−streptomycin in a humidified atmosphere of 5% CO_2 at 37 °C. The steps for telomerase extraction are as follows: 1×10^6 harvested cells were washed twice with ice-cold phosphate-buffered saline (PBS) solution. The cells were then resuspended in 200 μL of ice-cold CHAPS lysis buffer (composed of 10 mM Tris HCl, 0.1 mM PMSF, 1 mM EGTA, 1 mM $MgCl_2$, 5 mM 2-Hydroxy-1-ethanethiol, 0.5% CHAPS, 10% glycerol, pH 7.5) and incubated on ice for 30 min. Following centrifugation (12000 rpm, 30 min, 4 °C), the resulting supernatant was carefully transferred to a fresh EP tube and either utilized immediately or stored at −80 °C for subsequent use. In negative control experiments, cell extracts underwent heat treatment at 95 °C for 10 min to denature the telomerase activity.

Cell Cycle Synchronizations and Flow Cytometric Analysis. To synchronize Hela cells at different phases of the cell cycle, methods described in the literature were followed.[28,29] For synchronization at the G0/G1 phase, Hela cells were arrested by serum starvation. Specifically, the exponentially growing cells (1.0×10^6 cells) were plated in a 6-well culture plate with DMEM medium devoid of FBS. The cells were incubated at 37 °C for 24 h before harvesting. For Hela cells synchronization of G1/S, S, and G2/M phases, cells were first plated in a 6-well culture plate with DMEM containing 10% FBS and incubated at 37 °C until they reached 70% density. To synchronize at the G1/S and S phases, Hela cells were incubated with DMEM medium containing 2.5 mM L-mimosine and 2 mM thymidine for 16 h prior to harvest, respectively. For synchronization at the G2/M phase, cells were cultured by DMEM medium containing 30 ng/mL nocodazole for 16 h before harvesting. To evaluate the effectiveness of cell synchronization, flow cytometry was performed. The attached cells (1.0×10^6 cells) were trypsinized, washed three times with PBS, and fixed in 75% ethanol at 4 °C overnight. Subsequently, the fixed cells were centrifuged at 400 × g for 5 min, resuspended in PBS containing 2 mM EDTA and 50 μg/mL RNase A, and incubated at 37 °C for 10 min. Propidium iodide (0.02 mg/mL) was added to stain the DNA content, and the cells were incubated at 37 °C for 30 min. The synchronization of the cells was assessed using flow cytometric analysis (Beckman Coulter, USA), and the results were analyzed using FlowJo 10.6.2 software.

Quantitative Real-Time PCR Analysis. Quantification of intracellular TERT mRNA involves total RNA extraction, reverse transcription, and quantitative fluorescence PCR. The total RNAs were extracted with a Trizol Reagent Kit (Takara) according to the manufacturer's instructions. The cDNAs were synthesized according to the instructions provided with the cDNA reverse transcription kit (Sangon Biotech). Subsequently, the cDNAs were subjected to fluorescence quantitative PCR using the fast qPCR master mix kit (BBI Life Sciences Corporation), and the relative expression of the identified miRNAs was determined using the $2^{-\Delta\Delta}$Ct technique with β-actin as the internal standard. The primers used for the PCR amplifications are as follows: TERT gene (forward, 5′-ATGTCACGGAGACCACGTTT-3′; reverse, 5′-GCACC-CTCTTCAAGTGCTGT-3′) and β-actin gene (forward, 5′-GTCCACCGCAAATGCTTCTA-3′; reverse, 5′-TGCTG-TCACCTTCACCGTTC-3′).

Native Polyacrylamide Gel Electrophoresis. The telomerase activity in different cell cycle phases was subjected

https://doi.org/10.1021/acsomega.4c03653
ACS Omega 2024, 9, 37780−37788

Scheme 1. Schematic for Cell Cycle Analysis Based on Telomerase Activity: (a) Evaluation of Telomerase Activity at Different Cell Cycle Stages; (b) S-Phase Cells Sorted by Fluorescence Intensity of Telomerase Activity; (c) Process of MB Self-Assembly Activated by Telomerase to Achieve Multilevel Fluorescence Signal Amplification in ALTMAN System

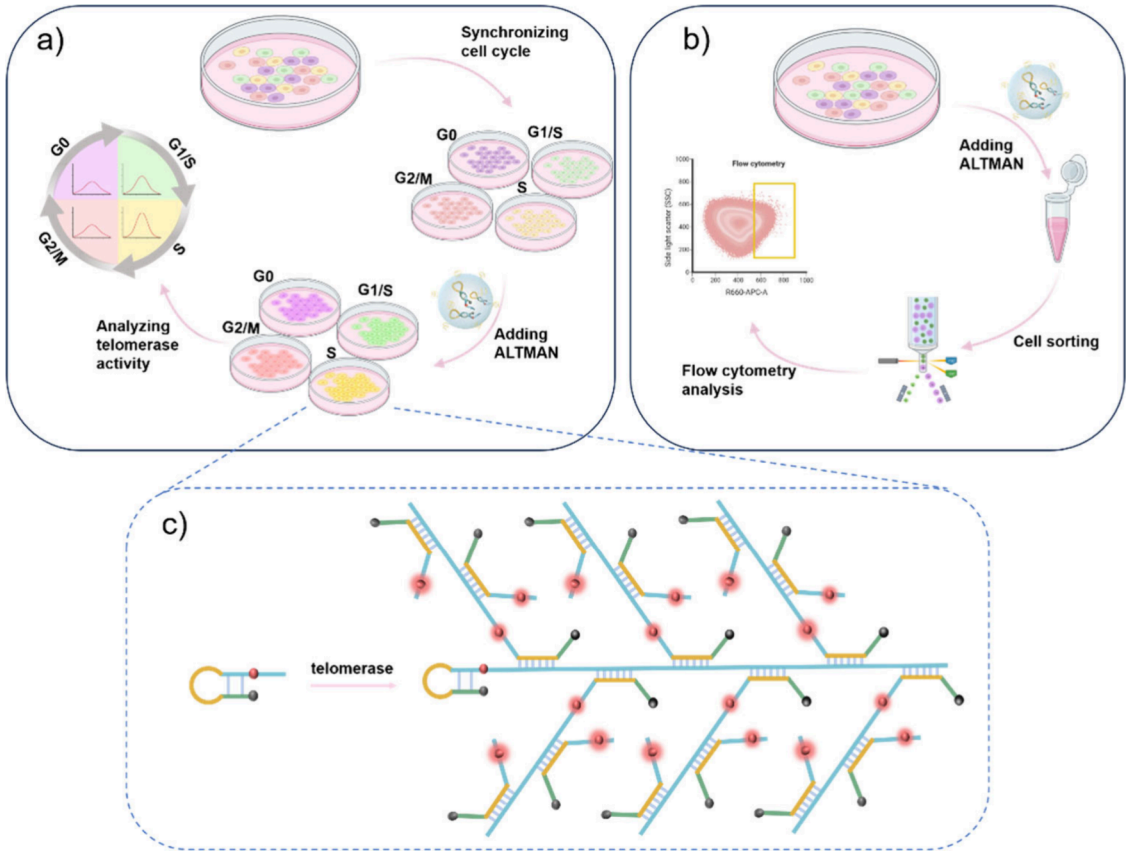

to characterization through 12% native polyacrylamide gel electrophoresis. 100 nM MB were incubated with telomerase extracted from cells (5×10^3 cells) in the reaction buffer containing 0.1 mM dNTP at 37 °C for 1 h. Then the resultant samples (10 μL) were mixed with 3 μL of DNA loading buffer and injected into the native polyacrylamide gel for electrophoresis. Electrophoresis was conducted in a 1 × Tris-borate-EDTA (TBE) buffer (comprising 89 mM Tris, 89 mM boric acid, and 2.0 mM EDTA, pH 8.3) at 110 V for 60 min. After the electrophoresis, the gels were stained with Gel Red (utilized at a dilution of 1:10,000, v/v) for 10 min and images of the gels were captured using a Bio-Rad fluorescence gel imaging system.

Evaluation of Telomerase Activity Extracted from Cells with Different Cell Cycles. The mixture comprising 100 nM MB, 0.1 mM dNTP, and varying concentrations of telomerase extracted from cells in different cell cycle stages, were prepared by combining them with the reaction buffer. Following an incubation period of 2 h at 37 °C, fluorescence spectra were systematically recorded within the range of 650 to 800 nm, utilizing an excitation wavelength of 634 nm.

***In Situ* Imaging of Telomerase Activity.** Cells were seeded into culture dishes and cultured at 37 °C for 24 h. After cell cycle synchronization, the telomerase activity assay system was added to the cells and incubated for 4 h. The cells were washed with PBS three times to remove the uninternalized probes and the cell nuclei were stained with DAPI for 5 min at 37 °C. Fluorescence imaging of the cells was conducted utilizing 63× objective lenses on the Zeiss LSM980 Airyscan microscope (Zeiss, Germany). The pumped diode lasers at 639 nm were used for the excitation of Cy5 and the excitation wavelength of DAPI was 405 nm. The confocal fluorescence images were subjected to processing through ImageJ software before presentation.

Flow Cytometry Sorting. Cells were seeded in a 6-well culture plate and cultured at 37 °C for 24 h. After removing the culture medium, cells were incubated with a culture medium containing the telomerase activity assay system. After 4 h of incubation at 37 °C, the cells were trypsinized. The cells were washed three times and then resuspended with PBS supplemented with 2% FBS. Aqua Live/Dead (ThermoFisher, L34957) was used to exclude dead cells in all experiments. After preprocessing the cell suspension to be tested, we first used FSC-A/SSC-A parameters to gate the target cell population. Next, we applied FSC-A/SSC-H parameters to exclude aggregated cells and obtain a single-cell population. Finally, we sorted the cells based on telomerase activity fluorescence intensity, selecting those with high fluorescence intensity as the experimental group, while the remaining cells were designated as the control group for subsequent validation experiments. Flow cytometry analysis was performed on a BD FACSAria III Cell Sorter instrument and analyzed using FCS Express 7.

Statistical Analysis. The data were expressed as the mean ± standard deviation. Statistical significance was assessed using the two-tailed Student's *t* test for comparisons involving two groups, or analysis of variance (ANOVA) for comparisons involving three or more groups conducted using GraphPad Prism 8.0.2. Statistical significance levels were denoted as follows: $^*P < 0.05$, $^{**}P < 0.01$, $^{***}P < 0.001$, $^{****}P < 0.0001$, ns: not significant.

https://doi.org/10.1021/acsomega.4c03653
ACS Omega 2024, 9, 37780−37788

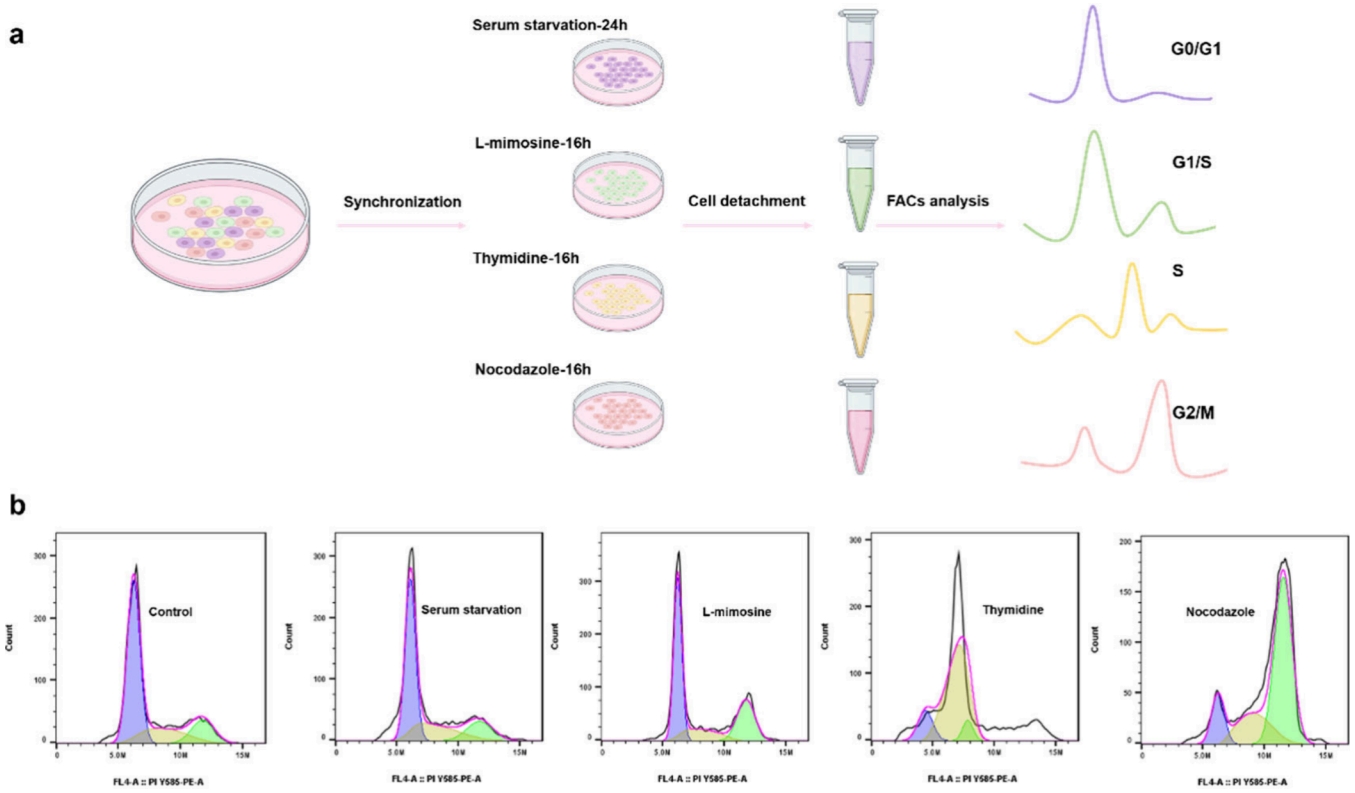

Figure 1. Hela cell cycle synchronization. (a) Schematic diagram of experimental procedure for cell cycle synchronization. (b) Flow cytometry analysis of cell cycle synchronization effect.

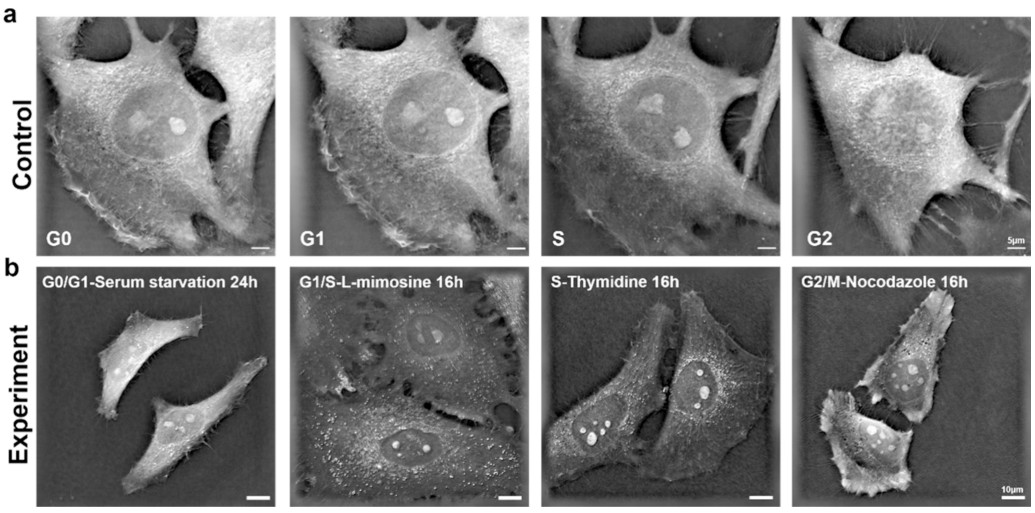

Figure 2. Morphology of living cells at different cell cycle stages observation by live cell microscopy. (a) Cell morphology of untreated Hela cells in G0/G1/S/G2 phase; (b) Cell morphology of cell cycle blocker-treated Hela cells at different cell cycle stages, Scale bar: 10 μm, 5 μm.

RESULTS AND DISCUSSION

Principle of the ALTMAN-Based Cell Cycle Analysis Strategy. We proposed a simple and effective method for S-phase identification based on ALTMAN telomerase activity analysis. The ALTMAN approach was an aptamer liposome-mediated telomerase-activated MB arborescent nano self-assembly system for real-time, high-fidelity detection of telomerase activity. The principle of ALTMAN was that intracellular telomerase-activated MB unfolded its hairpin structure and self-assembled to form arborescent structures, which realized the highly sensitive output of telomerase activity fluorescence signal. As shown in Scheme 1, the different cell cycle telomerase activities were analyzed via ALTMAN strategy and validated that the cells exhibited enhanced telomerase activity in the S phase, which laid the research foundation for subsequent cell cycle analysis based on telomerase activity. Next, we performed fluorescence flow sorting of telomerase activity by ALTMAN approach to determine the fluorescence intensity of S-phase cell sorting and to realize S-phase cell differentiation in cultured cells. In this manner, we successfully identified S-phase cells from the cultured cell population, which provided an effective new approach for subsequent S-phase-oriented assessment of tumor malignancy and therapeutic prognosis.

https://doi.org/10.1021/acsomega.4c03653
ACS Omega 2024, 9, 37780−37788

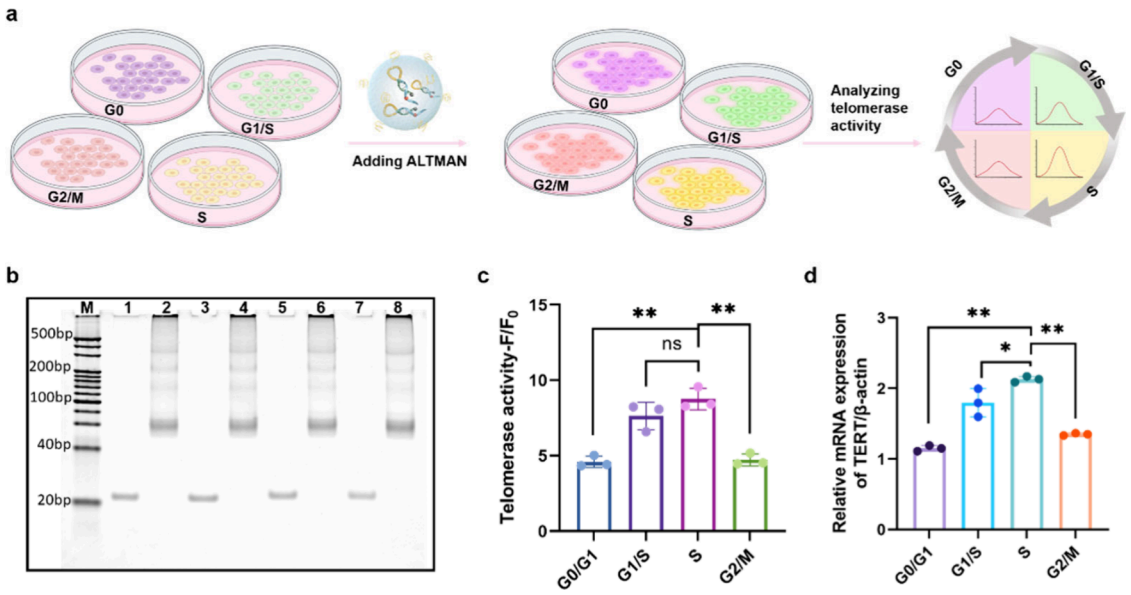

Figure 3. Performance evaluation of extracellular telomerase activity assay via MB. (a) Schematic representation of different cell cycle telomerase activities detected by MB. (b) Polyacrylamide gel electrophoretic analysis of telomerase-activated MB nanoscale self-assembly in different cell cycles (G0/G1, G1/S, S and G2/M). Lane 1: MB; Lane 2: MB+G0/G1-TE; Lane3: MB; Lane 4: MB+G1/S-TE; Lane 5: MB; Lane 6: MB+S-TE; Lane 7: MB; Lane 8: MB+G2/M-TE. (c) Assay of extracellular telomerase activity in different cell cycle phases. (d) qPCR analysis of telomerase reverses transcription protein TERT mRNA gene expression levels in different Hela cell cycle phases. Data are means = SD (n = 3). *P < 0.05; **P < 0.01; ns, not significant.

Validation of Cell Cycle Synchronization. First, Hela cells were subjected to cell cycle synchronization to investigate the correlation between telomerase activity and cell cycle progression. Hela cells were treated with serum starvation, L-mimosine, Thymidine, and Nocodazole at different time, resulting in cell arrests at G0/G1, G1/S, S, and G2/M phases, respectively (Figure1a). The efficacy of synchronization was determined by flow cytometry analysis of intracellular DNA content at each cell cycle phase (Figure 1b). The results showed that most of the Hela cells treated with different methods were blocked at the corresponding cell cycle phase (Figure S1).

Next, live cell imaging microscopy was employed to observe the morphology of cells under distinct treatments. We observed the cellular state of untreated Hela cells at different cell cycle stages. During the progression of the Hela cell cycle, chromatin in the nucleus gradually began to condense in preparation for division (Figure 2a). As shown in Figure 2b, when the cells were blocked at the G0/G1 phase by serum starvation treatment for 24 h, the cell volume was obviously wrinkled due to serum-deficient culture, and the intracellular lipid droplets were not obvious. L-mimosine treatment for 16 h caused cell arrest in the G1/S phase, inducing a significant increase in cell volume and a flattened cell shape. The cell morphology of Thymidine-treated cells in the S phase was not significantly different from that of the G1/S phase, and the nuclei were clearly defined. After Nocodazole treatment for 16 h to block the cells in the G2/M phase, the intracellular nuclei began to blur and gradually formed spindle bodies. In addition, we also observed the cellular state during the cell cycle progression in live cells under time series, in keeping with the above results (Movies S1−S5). The results indicated that we successfully blocked the cells at the corresponding cell cycle by different cell cycle blockers.

Evaluation of Extracellular Telomerase Activities via MB. We analyzed the extracted telomerase activity from cells in different cell cycle phases (Figure 3a). Polyacrylamide gel electrophoresis (PAGE) experiments confirmed that MB could be extended by telomerase activation at various cell cycle stages (Figure 3b). Fluorescence spectroscopy was employed to assess the telomerase activity in different cell cycles. The telomerase activity exhibited low levels in the G0/G1 and G2/M cell cycle phases, while enhanced fluorescence signals were presented in the G1/S and S phases (Figure 3c). We also analyzed the TERT mRNA expression in cells of different cell cycle phases by quantitative real-time PCR. The TERT mRNA expression level was lower in the G0/G1 and G2/M phases, and higher in the G1/S and S phases (Figure 3d), which was also consistent with the results of the above analysis of telomerase activity. The results of the above experiments indicated that telomerase activity was subject to cell cycle progression-dependent changes and was found to have the strongest active expression level in the S phase. The reason for this may lie in the fact that telomerase was a protease that was specifically activated in malignant cells, and in the presence of telomerase, most malignant cells could maintain telomeres in the S-phase of the cell cycle. In particular, telomerase activity could be regenerated by up-regulation of the expression level of TERT mRNA in different types of human malignant tumors. All of the above results indicated that our assay system successfully achieved a positive correlation between TERT mRNA and telomerase activity and fluorescence intensity, revealing the differences in the expression levels of tumor markers under different cell cycles.

Validation of Intracellular Telomerase Activity in Different Cell Cycle Phases. To ensure that there was no leakage or interference from a nonspecific fluorescent background during intracellular imaging, we performed a stability analysis of MB. We simulated the intracellular environment in which MB might be present, including cell lysate, DNAzyme I, cell cycle blockers (L-mimosine, Thymidine, Nocodazole), and buffers of different pH (4−8) to verify the stability of MB for intracellular analysis. As shown in Figure S2a, following coincubating MB with various buffers and cell cycle blockers at different time, the fluorescence of MB increased insignif-

https://doi.org/10.1021/acsomega.4c03653
ACS Omega 2024, 9, 37780−37788

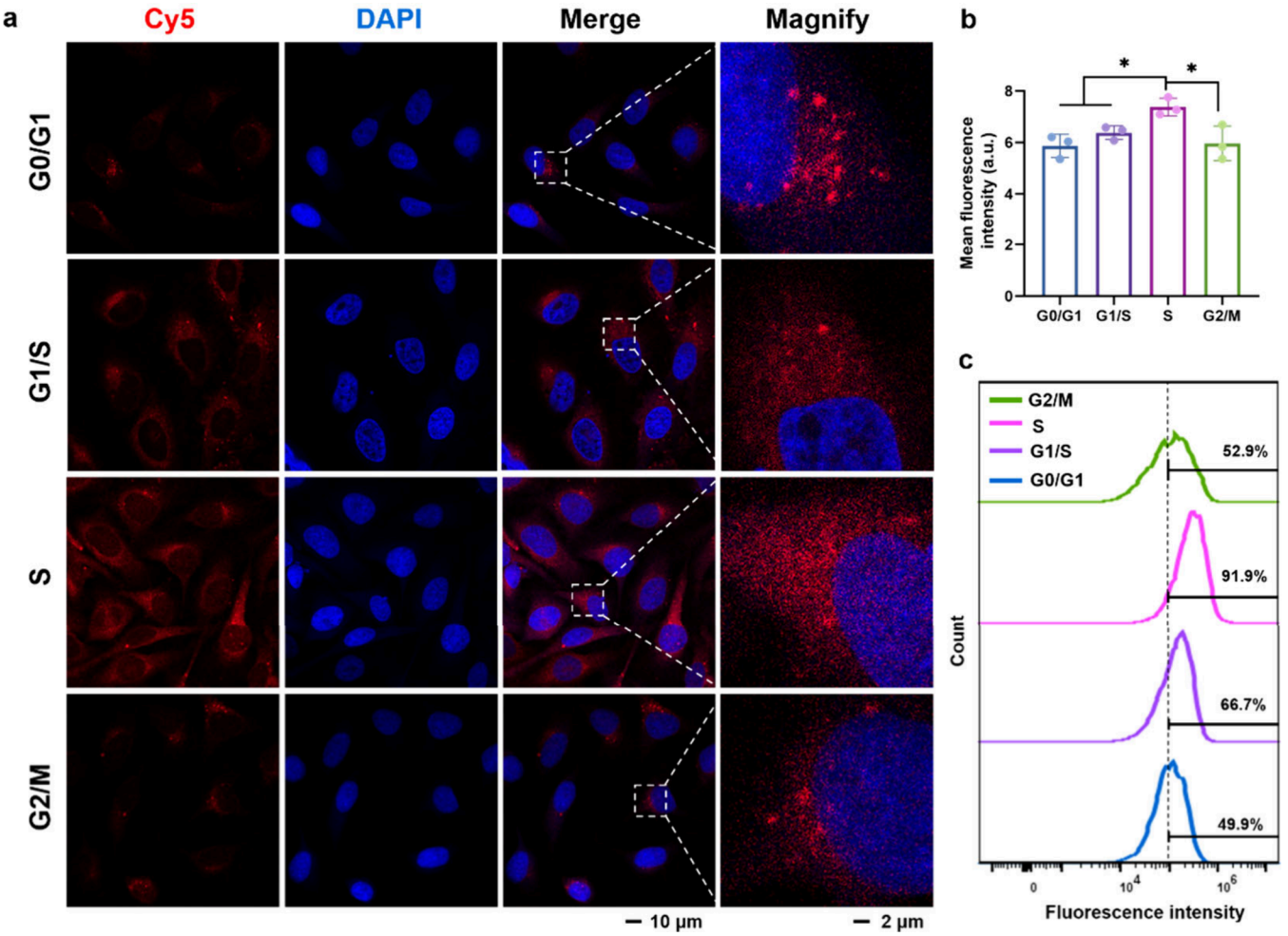

Figure 4. Validation of intracellular telomerase activity in different cell cycle phases. (a) Confocal fluorescence images of telomerase activity in Hela cells at different cell cycle phases. Scale bar: 10 μm, 2 μm. (b) Relevant statistical histogram analysis of the CLSM images. (c) Flow cytometric assay of telomerase activity in Hela cells at different cell cycle phases. Data are means ± SD (n = 3). Statistical significance was calculated via Student's t test. *P < 0.05.

icantly, confirming its stability in various buffers and cell cycle blockers. Furthermore, no substantial enhancement in the fluorescence intensity of MB was observed after coincubation with buffers at different pH levels for 0−24 h, affirming the robust stability of MB in intracellular bioassays (Figure S2b). Next, we evaluated the capability of MB for the analysis of telomerase activity in tumor cell lines. The malignant tumor cell line (Hela, MCF-7) and a control normal somatic cell line (HL-7702) were reacted with MB, respectively. Intracellular telomerase fluorescence imaging was observed by confocal microscopy, which showed a strong Cy5 fluorescence signal in the malignant tumor cell line, while the fluorescence signal was almost invisible in the normal somatic cells (Figure S3a). ImageJ software was employed for analyzing the average fluorescence intensity in live cells showed a consistent trend of Cy5 signal changes (Figure S3b). In addition, we also analyzed the Cy5 fluorescence intensity of telomerase activity of the above cells under MB analysis by flow cytometry, and the results exhibited great agreement with the confocal images (Figure S3c). The above experimental results confirmed the excellent performance of MB for *in situ* intracellular telomerase activity analysis.

After validating the basic intracellular telomerase activity assay performance of MB, we investigated telomerase activities within *in situ* cells across different cell cycle phases. Cells were arrested at G0/G1, G1/S, S, and G2/M phases, and subsequently MB was reacted with the above cells. The confocal fluorescence images illustrated the variations in telomerase activity among cells in different cell cycles, with an enhanced fluorescence signal observed particularly in the S phase (Figure 4a, 4b). We also analyzed the fluorescence intensity of telomerase activity in different cell cycles by flow cytometry. One $\times 10^5$ was used the analytical standard to compare the intracellular telomerase fluorescence intensity of each cell cycle phase, the results demonstrated that S-phase cells had stronger fluorescence intensity than cells in other cycle stages (Figure 4c). The flow fluorescence intensity of 1×10^5 was employed as a reference of fluorescence intensity for preliminary flow sorting of S-phase cells.

S-Phase Cell Sorting Based on Telomerase Activity. The preceding experiments demonstrated a correlation between telomerase activity and cell cycle progression, particularly an increase in intracellular telomerase activity in S-phase cells. Therefore, we tried to analyze whether the cells were mostly in the S phase by assessing intracellular telomerase activity. We added the telomerase activity detection system ALTMAN to the cultured cells and assessed the fluorescence signal intensity of telomerase activity using a flow cell sorting instrument (Figure 5a). Based on the results of the flow cell fluorescence intensity

https://doi.org/10.1021/acsomega.4c03653
ACS Omega 2024, 9, 37780−37788

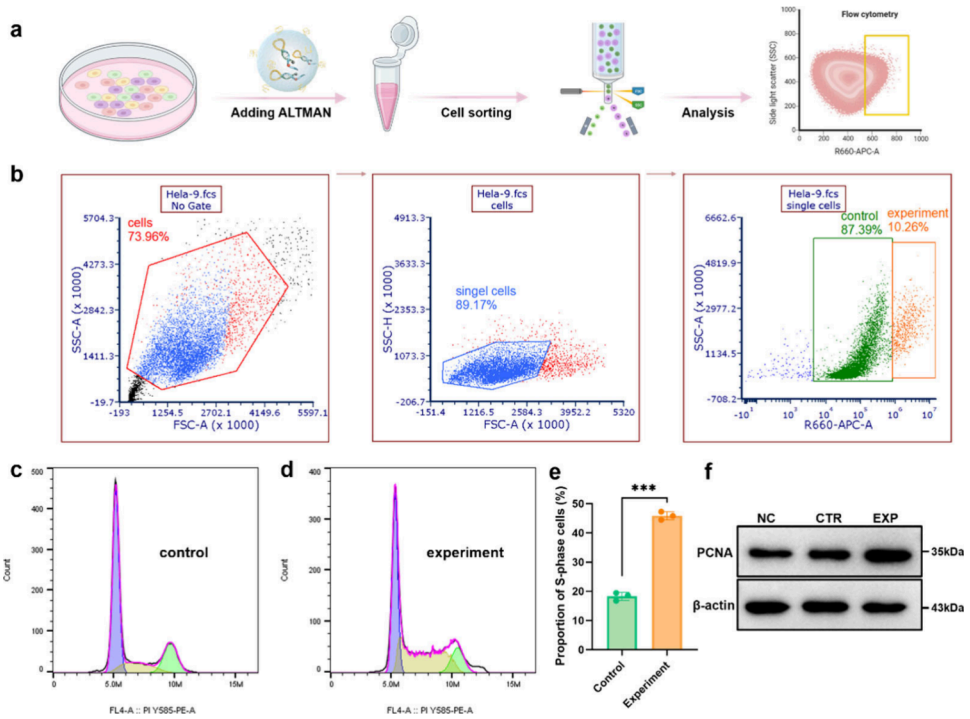

Figure 5. S-phase cell sorting based on telomerase activity. (a) Schematic illustration of S-phase cells sorted by fluorescence intensity of telomerase activity. (b) Flow cytometric analysis process of S-phase cells based on fluorescence intensity of telomerase activity. (c, d) Flow cytometric cycle analysis of two groups of sorted cells (experimental and control). (e) Stacked Histogram of cell cycle flow analysis of two groups of sorted cells. (f) Western blotting analysis of PCNA protein expression of normal (NC), control (CTR), and experiment (EXP) cells. Data are means ± SD (n = 3). Statistical significance was calculated via Student's t test. ***$P < 0.001$.

analysis, we finally determined to use 1×10^6 as the fluorescence intensity for the sorting of S-phase cells (Figure 5b). We analyzed the cell viability of the experimental and control cells obtained by flow cytometric sorting using MTT assay. The results showed that the cell viability of normal untreated cells was about 90%, and the cell viability of the experimental and control groups was about 70% (Figure S4). This result indicated that the cell-sorted cells maintained certain cell viability and can be used for further experimental research, although the cell viability decreased compared to that of normal untreated cells.

To verify whether most of our sorted cells were in S-phase, we analyzed the sorted experimental group and control group separately by using flow cytometry cell cycle assay (Figure 5c, 5d). The proportion of cells in the S-phase in the experimental group was significantly higher than that in the control group. Stacked histograms also showed consistent results (Figure 5e). Subsequently, we conducted a statistical analysis of the S-phase proportions of the cells in the two groups, and the results showed that the S-phase proportions of the cells in the two groups were significantly different (Figure S5). Proliferating Cell Nuclear Antigen (PCNA) was a protein abundantly expressed during the proliferation phase of the cell cycle, with its expression level being relatively high during the S phase. We analyzed PCNA protein expression levels in the two groups of cells to corroborate whether the cells sorted using our method were predominantly in the S phase. The results in Figure 5f showed a significantly higher expression level of the PCNA protein in the experimental group cells compared to both the control cells and normal untreated cells. Furthermore, quantitative analysis of the PCNA protein expression levels corroborated these results (Figure S6). Therefore, the above results indicated that the S-phase of cells could be effectively sorted out based on telomerase activity analysis via ALTMAN. The successful cell cycle S-phase sorting achieved through telomerase activity analysis underscored the potential of this approach for precise and efficient cell cycle studies and sorting strategies.

CONCLUSIONS

In summary, we performed a simple and effective S-phase cell assay approach that allows precise differentiation of S-phase cells in a cell population by measuring real-time intracellular telomerase activity in different cell cycles using the ALTMAN method. This technique provides unique insights into the field of single-cell analysis assays and demonstrates certain advantages. Specifically, the method effectively avoids the limitations of traditional DNA ploidy-based fluorescent dyes and flow analysis of S-phase cells, such as the confusion of DNA ratios and the high cytotoxicity of fluorescent dyes, and ensures the precision of S-phase cell differentiation. Through real-time dynamic analysis of intracellular telomerase activity of cultured cells, this approach successfully distinguished S-phase cells with certain sensitivity and specificity. Moreover, we have experimentally verified that the cells after cell cycle analysis by this method still maintain high cell viability. Another advantage of ALTMAN technology for cell cycle analysis is the use of a red fluorescent probe, which offers a strong tissue penetration ability, and is conducive to tumor-related studies based on cell cycle analysis. The S-phase cell analysis based on telomerase activity introduces a novel approach to single-cell cycle analysis. Moreover, evaluating the fraction of S-phase cells presents a new pathway for assessing tumor malignancy and treatment prognosis in tumor patients.

https://doi.org/10.1021/acsomega.4c03653
ACS Omega 2024, 9, 37780−37788

■ ASSOCIATED CONTENT

Supporting Information

The Supporting Information is available free of charge at https://pubs.acs.org/doi/10.1021/acsomega.4c03653.

Movie of the untreated Hela cell status during the cell cycle progression under time series (ZIP)

Movie of cell status under time series after serum starvation treatment for 24 hours to block Hela cells in G0/G1 phase (ZIP)

Movie of cell status under time series after L-mimosine treatment for 16 hours to block Hela cells in G1/S phase (ZIP)

Movie of cell status under time series after Thymidine treatment for 16 hours to block Hela cells in S phase (ZIP)

Movie of cell status under time series after Nocodazole treatment for 16 hours to block Hela cells in G2/M phase (ZIP)

Results of flow cytometry analysis, stability of MB, intracellular telomerase activity analysis in different cell lines, cell viability evaluation, cell cycle stacked histogram of sorted cells, and protein quantification analysis (PDF)

■ AUTHOR INFORMATION

Corresponding Authors

Yang Luo − *Center of Smart Laboratory and Molecular Medicine, School of Medicine and NHC Key Laboratory of Birth Defects and Reproductive Health, Chongqing University, Chongqing 400044, People's Republic of China;* orcid.org/0000-0002-0166-9027; Email: luoy@cqu.edu.cn

Wei Gu − *Center of Smart Laboratory and Molecular Medicine, School of Medicine, Chongqing University, Chongqing 400044, People's Republic of China;* orcid.org/0000-0002-9529-4683; Email: guwei@cqu.edu.cn

Authors

Zining Wang − *Center of Smart Laboratory and Molecular Medicine, School of Medicine, Chongqing University, Chongqing 400044, People's Republic of China*

Tian Wang − *Center of Smart Laboratory and Molecular Medicine, School of Medicine, Chongqing University, Chongqing 400044, People's Republic of China*

Xiaohui Chen − *Department of Clinical Laboratory, Fuling Hospital, Chongqing University, Chongqing 408099, People's Republic of China; NHC Key Laboratory of Birth Defects and Reproductive Health, Chongqing University, Chongqing 400044, People's Republic of China*

Linxi Lv − *Center of Smart Laboratory and Molecular Medicine, School of Medicine, Chongqing University, Chongqing 400044, People's Republic of China*

Complete contact information is available at: https://pubs.acs.org/10.1021/acsomega.4c03653

Author Contributions

The study was conceived and the experiments were designed by Z.W., W.G., and Y.L. Z.W. and X.C. carried out the experimental sample preparations. The experiments were performed by Z.W., T.W., and L.L. Z.W., X.C., and T.W. analyzed the experimental data. Z.W., W.G., and Y.L. wrote and revised the manuscript. All authors reviewed and approved the manuscript.

Funding

This work was supported by the Natural Science Foundation of Chongqing, China (No.CSTB2023NSCQ-MSX1038), the National Natural Science Foundation of China (No.82372549, 82125022), and Yunnan Province major science and technology special project "biomedical field" project (No. 202302AA310039).

Notes

The authors declare no competing financial interest.

■ ACKNOWLEDGMENTS

We thank the staff of the Medical Experimental Center of School of Medicine, Chongqing University, for technical assistance.

■ REFERENCES

(1) Coffman, J. A. Cell Cycle Development. *Developmental Cell* **2004**, *6* (3), 321−327.

(2) Rao, P. N.; Johnson, R. T. Mammalian Cell Fusion: Studies on the Regulation of DNA Synthesis and Mitosis. *Nature* **1970**, *225* (5228), 159−164.

(3) Hartwell, L. H.; Kastan, M. B. Cell Cycle Control and Cancer. *Science* **1994**, *266* (5192), 1821−1828.

(4) Johnson, R. T.; Rao, P. N. Mammalian Cell Fusion: Induction of Premature Chromosome Condensation in Interphase Nuclei. *Nature* **1970**, *226* (5247), 717−722.

(5) Xiong, W.; Jiao, Y.; Huang, W.; Ma, M.; Yu, M.; Cui, Q.; Tan, D. Regulation of the Cell Cycle via Mitochondrial Gene Expression and Energy Metabolism in HeLa Cells. *ABBS* **2012**, *44* (4), 347−358.

(6) Sclafani, R. A.; Holzen, T. M. Cell Cycle Regulation of DNA Replication. *Annual Review of Genetics* **2007**, *41* (1), 237−280.

(7) Laskey, R. A.; Fairman, M. P.; Blow, J. J. S Phase of the Cell Cycle. *Science* **1989**, *246* (4930), 609−614.

(8) Shaw, A.; Olivares-Chauvet, P.; Maya-Mendoza, A.; Jackson, D. A. S-Phase Progression in Mammalian Cells: Modelling the Influence of Nuclear Organization. *Chromosome Res.* **2010**, *18* (1), 163−178.

(9) Malm, C.; Jaremko, G.; Brehmer, M. S-Phase − an Independent Prognostic Marker in Upper Tract Urothelial Carcinoma. *Scandinavian Journal of Urology* **2022**, *56* (5−6), 397−403.

(10) Yan, N.; Tang, B. Z.; Wang, W.-X. Cell Cycle Control of Nanoplastics Internalization in Phytoplankton. *ACS Nano* **2021**, *15* (7), 12237−12248.

(11) Liu, J.; Peng, Y.; Wei, W. Cell Cycle on the Crossroad of Tumorigenesis and Cancer Therapy. *Trends in Cell Biology* **2022**, *32* (1), 30−44.

(12) Ligasová, A.; Frydrych, I.; Koberna, K. Basic Methods of Cell Cycle Analysis. *International Journal of Molecular Sciences* **2023**, *24* (4), 3674.

(13) Slater, M. L.; Sharrow, S. O.; Gart, J. J. Cell Cycle of Saccharomycescerevisiae in Populations Growing at Different Rates. *Proc. Natl. Acad. Sci. U. S. A.* **1977**, *74* (9), 3850−3854.

(14) Clinical Practice Guidelines for the Use of Tumor Markers in Breast and Colorectal Cancer. Adopted on May 17, 1996 by the American Society of Clinical Oncology. *J. Clin Oncol* **1996**, *14* (10), 2843−2877.

(15) Shankey, T. V.; Rabinovitch, P. S.; Bagwell, B.; Bauer, K. D.; Duque, R. E.; Hedley, D. W.; Mayall, B. H.; Wheeless, L.; Cox, C. Guidelines for Implementation of Clinical DNA Cytometry. International Society for Analytical Cytology. *Cytometry* **1993**, *14* (5), 472−477.

(16) Kim, K. H.; Sederstrom, J. M. Assaying Cell Cycle Status Using Flow Cytometry. *CP Molecular Biology* **2015**, *111* (1), 1.

(17) Bialic, M.; Al Ahmad Nachar, B.; Koźlak, M.; Coulon, V.; Schwob, E. Measuring S-Phase Duration from Asynchronous Cells Using Dual EdU-BrdU Pulse-Chase Labeling Flow Cytometry. *Genes* **2022**, *13* (3), 408.

(18) Eidukevicius, R.; Characiejus, D.; Janavicius, R.; Kazlauskaite, N.; Pasukoniene, V.; Mauricas, M.; Otter, W. D. A Method to Estimate Cell

Cycle Time and Growth Fraction Using Bromodeoxyuridine-Flow Cytometry Data from a Single Sample. *BMC Cancer* **2005**, *5* (1), 122.
(19) Takahashi, K.; Tanabe, R.; Ehata, S.; Kubota, S. I.; Morishita, Y.; Ueda, H. R.; Miyazono, K. Visualization of the Cancer Cell Cycle by Tissue-Clearing Technology Using the Fucci Reporter System. *Cancer Science* **2021**, *112* (9), 3796−3809.
(20) Pennycook, B. R.; Vesela, E.; Peripolli, S.; Singh, T.; Barr, A. R.; Bertoli, C.; de Bruin, R. A. M. E2F-Dependent Transcription Determines Replication Capacity and S Phase Length. *Nat. Commun.* **2020**, *11* (1), 3503.
(21) Charrasse, S.; Gharbi-Ayachi, A.; Burgess, A.; Vera, J.; Hached, K.; Raynaud, P.; Schwob, E.; Lorca, T.; Castro, A. Ensa Controls S-Phase Length by Modulating Treslin Levels. *Nat. Commun.* **2017**, *8* (1), 206.
(22) Dhaene, K.; Van Marck, E.; Parwaresch, R. Telomeres, Telomerase and Cancer: An up-Date. *Virchows Arch* **2000**, *437* (1), 1−16.
(23) Srinivas, N.; Rachakonda, S.; Kumar, R. Telomeres and Telomere Length: A General Overview. *Cancers (Basel)* **2020**, *12* (3), 558.
(24) Londoño-Vallejo, J. A.; Wellinger, R. J. Telomeres and Telomerase Dance to the Rhythm of the Cell Cycle. *Trends Biochem. Sci.* **2012**, *37* (9), 391−399.
(25) Chen, L.; Jiao, Y.; Guan, X.; Li, X.; Feng, Y.; Jiao, M. Investigation of Cell Cycle-Associated Structural Reorganization in Nucleolar FC/DFCs from Mouse MFC Cells by Electron Microscopy. *Microscopy* **2018**, *67* (4), 222−231.
(26) Zhu, X.; Kumar, R.; Mandal, M.; Sharma, N.; Sharma, H. W.; Dhingra, U.; Sokoloski, J. A.; Hsiao, R.; Narayanan, R. Cell Cycle-Dependent Modulation of Telomerase Activity in Tumor Cells. *Proc. Natl. Acad. Sci. U. S. A.* **1996**, *93* (12), 6091−6095.
(27) Wang, Z.; Chen, X.; Qiu, X.; Chen, Y.; Wang, T.; Lv, L.; Guo, X.; Yang, F.; Tang, M.; Gu, W.; Luo, Y. High-Fidelity Sensitive Tracing Circulating Tumor Cell Telomerase Activity. *Anal. Chem.* **2024**, *96* (14), 5527−5536.
(28) Yoshizawa-Sugata, N.; Masai, H. Cell Cycle Synchronization and Flow Cytometry Analysis of Mammalian Cells. In *Cell Cycle Control*; Noguchi, E., Gadaleta, M. C., Eds. Springer New York: 2014; Methods in Molecular Biology, Vol. *1170*, pp 279−293.
(29) Eriksson, D.; Löfroth, P.-O.; Johansson, L.; Riklund, K. Å.; Stigbrand, T. Cell Cycle Disturbances and Mitotic Catastrophes in HeLa Hep2 Cells Following 2.5 to 10 Gy of Ionizing Radiation. *Clin. Cancer Res.* **2007**, *13* (18), 5501s−5508s.

https://doi.org/10.1021/acsomega.4c03653
ACS Omega 2024, 9, 37780−37788